Tellus (2003), 55A, 88–105
Printed in UK. All rights reserved

Copyright © Blackwell Munksgaard, 2003
TELLUS
ISSN 0280–6495

Examination of the sensitivity of forecast precipitation rates to possible perturbations of initial conditions

By RONALD M. ERRICO[1]*, KEVIN D. RAEDER[1] and LUC FILLION, [1]*National Center for Atmospheric Research, Boulder, Colorado, USA;* [2]*Canadian Meteorological Center, Montreal, Canada*

(Manuscript received 12 October 2001; in final form 3 July 2002)

ABSTRACT

An adjoint model that includes precipitation physics is applied to four synoptic cases in order to compare the sensitivities of both convective and non-convective precipitation rates with respect to initial perturbations of temperature, water vapor mixing ratio, vorticity or divergence. These are contrasted with sensitivities of barotropic vorticity. Forecast periods between 1 and 24 h are investigated. Root-mean-square values of the sensitivities as a function of vertical coordinate and field are presented as well as time series of impacts of optimal perturbations weighted by initial variances of uncertainties in the fields. For all the forecast aspects and cases considered, the greatest sensitivity and impacts are with regard to the temperature field. Precipitation is equally sensitive to vorticity and divergence, but when their relative uncertainties are considered, impacts of the vorticity dominate those of divergence. Precipitation is sensitive to initial specific humidity, but so is barotropic vorticity within a cyclone. The sensitivities of precipitation were not found to increase with forecast periods as much as the sensitivities to vorticity, suggesting that even within the same synoptic feature, different processes are responsible for the development of these distinct characteristics. Although comparison with corresponding impacts in the nonlinear model suggests that a 24 h period is too long for the adjoint-estimated precipitation impacts to be good approximations to the nonlinear results in some of the cases, 6-h adjoint-estimated results appear useful.

1. Introduction

For many purposes it is important to know the relative sensitivities of some forecast aspect with respect to different initial fields. For example, as a first attempt to assimilate accumulated precipitation data, how appropriate is it to ignore adjustments of temperature and wind compared with those of moisture? Or, for short-term forecasts of cyclonic storms, what potential effects can initial errors of moisture or velocity divergence have compared with errors in temperature or vorticity? Can initial moisture perturbations be ignored in estimating the mean predictability of the atmosphere? Answers to such questions are often critical to making rational decisions regarding data assimilation and to increasing understanding of atmospheric behavior in general.

Many sensitivity studies have been reported in the literature, but most have been conducted using forward models that propagate specified initially perturbed fields in time (e.g., Anthes et al., 1985; Errico and Baumhefner, 1987; Mullen and Baumhefner, 1989; Stensrud et al., 2000, and references therein). Comparison with an unperturbed forecast is interpreted as a sensitivity. Such results are more properly interpreted as impacts, however, with little revealed about the sensitivity with respect to other perturbations not explicitly examined. Indeed, such results can be misleading concerning the sensitivity of other, unexamined, initial perturbation structures (see, e.g., Langland et al., 1995; 1996; Lewis et al., 2001).

*Corresponding author. Address: Data Assimilation Office, NASA/GSFC, Code 910.3, Greebelt, MD, 20771, USA. e-mail: rerrico@dao.gsfc.nasa.gov

Another method of determining sensitivities is to use a model's adjoint (e.g., Hall et al., 1982; Errico, 1997). The adjoint, derived from a forecast model, efficiently propagates sensitivities of scalar functions of the forecast model's output backwards in time to determine corresponding sensitivities with respect to the model's input (e.g., values of initial or boundary conditions). If interest is focused on only a small number of measures of aspects of a model forecast, then only that number of executions of the adjoint model are necessary in order to determine their sensitivity with respect to all possible perturbations of every input variable. The limitation of this approach is that the sensitivities obtained yield only linear estimates of potential impacts. For sufficiently large perturbation magnitudes or highly nonlinear and perhaps discontinuous physical equations, therefore, the adjoint results may also be misleading (Errico and Raeder, 1999). For an introduction to adjoint models and their uses, see Errico (1997).

Attention in this report is focused on sensitivities of forecasts of either precipitation rates or barotropic cyclonic vorticity with respect to model initial fields. The latter is considered primarily to contrast the sensitivity of a dynamic field to that of precipitation. The initial fields considered are the vertical component of vorticity, horizontal wind divergence, temperature and water-vapor mixing ratio. Magnitudes of sensitivities are examined as functions of the model vertical coordinate. Ranking of the sensitivities is performed by considering optimal structures having amplitudes consistent with crude estimates of the uncertainty of the initial fields. Our objective is focused on these magnitudes and rankings, but not on the synoptic interpretations of the sensitivity fields.

The forecast model and the forecast aspects investigated are both described in section 2, followed by a brief description of the examined synoptic cases in section 3. The resulting magnitudes of sensitivity fields are described in section 4 and the rankings of different fields in terms of optimal perturbations are described in section 5. In section 6, the validity of the linearization upon which the adjoint results are based is examined. Conclusions are presented in section 7.

2. Model and forecast aspects

The model used here is the Mesoscale Adjoint Modeling System (denoted as MAMS2) described in Errico and Raeder (1999). Pertinent details are that it uses the primitive equations defined using $\sigma = (p - p_t)/(p_s - p_t)$ as the vertical coordinate, where p is pressure, p_t is the model top and p_s is the surface pressure. At the model's top and surface, the σ-coordinate velocity ($\dot{\sigma}$) is specified as 0. Prognostic fields are defined within a regional domain on a Lambert conformal horizontal grid on 20 σ-levels (in addition to the surface), each with an equal thickness $\Delta\sigma = 0.05$. Horizontal resolution varies with the case investigated, as described later. Lateral boundaries are modeled using a Davies and Turner (1977) relaxation scheme acting within eight points of the grid edges. Time steps are centered differences except for the initial step that is forward in time. Dry diabatic processes include vertical and horizontal diffusion, bulk formulation of the planetary boundary layer, dry convective adjustment and a prognostic surface temperature over land. Moist diabatic processes include convective (Moorthi and Suarez, 1992) and stratiform precipitation and effects of relative-humidity determined clouds on radiation at the surface. A nonlinear vertical mode initialization scheme (Bourke and McGregor, 1983) is applied to the first two vertical modes. The model's adjoint version is exact except for some minor approximations applied for computational efficiency as described in Errico and Raeder (1999). See Errico et al. (1994) for full description of its parent model (MAMS1).

The model initial conditions include three-dimensional fields of vector wind components (**V**), temperature (T) and water-vapor mixing ratio (q), and two-dimensional fields of p_s and surface temperature. Here we shall consider the wind in terms of its vertical component of vorticity (ζ) and horizontal divergence (δ). Only sensitivities with respect to the three-dimensional fields are investigated.

All the forecast aspects are measured at the end of a 24-h model prediction. This end time is denoted hour 0, in accordance with the convention used for adjoint sensitivities by Errico and Vukićević (1992), so that the sensitivity fields refer to prior times $t \leq 0$. The units of t will be hours, so that an expression such as $-t > 6$ refers to possible initial times 6 h or longer before the end of the forecast.

Sensitivities at various times prior to the end of the forecast are determined in a single execution of the adjoint model. At each desired adjoint output time, the adjoint field values are saved and then the adjoint of a forward step and vertical mode initialization are executed and output. Subsequently, the backward-in-time adjoint execution continues by retrieving the saved values and proceeding with the adjoint of a centered time step. By this formulation, the sensitivities at intermediate times are exactly as though a forecast were to begin at that time. The one discrepancy is that the trajectory used for the adjoint's linearization is the original one produced by the nonlinear model for the forecast beginning at $t = -24$ h rather than one beginning somewhere $0 > t > -24$. For any experiment, the sensitivities denoted for any time are for forecasts ending at the same $t = 0$.

One forecast aspect considered is an area-mean barotropic vorticity determined for a box specified by all pairs of horizontal grid indices $i = i_1, \ldots, i_2$, $j = j_1, \ldots, j_2$. This aspect is computed as

$$J_\zeta = \frac{1}{N} \sum_{i=i_1}^{i_2} \sum_{j=j_1}^{j_2} \sum_{k=1}^{K} \zeta_{i,j,k}(t = 0)\Delta\sigma, \tag{2.1}$$

where $N = (i_2 - i_1 + 1)(j_2 - j_1 + 1)$ is the number of horizontal grid points in the selected area. According to Stoke's theorem, at $t = 0$ this J is only sensitive to wind components tangent to the sides of the box. Thus, sensitivities with respect to earlier times only concern possible effects of perturbations on the subsequent forecast of those particular wind components.

The rates of convective and non-convective precipitation at the surface at $t = 0$ are denoted as R_C and R_N, respectively. The other primary forecast aspects considered are area–mean values of these rates, denoted respectively as J_C and J_N. These means are computed over a contiguous subset of grid points as indicated in some following figures.

In taking the area-mean, the horizontal areas associated with each grid point are treated as though they are identical. On the MAMS2 grid, they are not actually equal, but nearly so (varying by less than 5% from the mean grid-box area). For convenience, those variations are neglected, both in defining any of the Js and in presenting sensitivity fields. Since the grid spacing $\Delta\sigma$ is k-independent, the vertical grid spacing is also neglected in presenting values of the sensitivity fields. For the MAMS2 grids used here, this is a good approximation to a norm defined by an integral over horizontal area and σ. For further discussion of the motivation for this implied norm, see Lewis et al. (2001).

3. Case descriptions

Four synoptic cases are examined. Two are winter cases and two are summer ones. All four have significant precipitation occurring within their domains. The cases are chosen for their differences, particularly regarding their dynamics, rather than their similarities, in order to enhance the likelihood of obtaining a range of results that would be more comprehensive than perhaps otherwise.

Case W1 is a 24-h forecast beginning 0000 UTC 14 February 1982. It is dominated by an explosively deepening cyclone off the Atlantic Coast of North America. This is the same case whose leading singular vectors are described in Ehrendorfer et al. (1999), Errico and Raeder (1999) and Errico (2000a; 2000b), except produced with twice the vertical resolution here. The horizontal grid spacing is $\Delta x = 120$ km and $p_\mathrm{t} = 10$ hPa.

Case W2 is a 24-h forecast beginning 1200 UTC 11 January 1996. Like case W1, it produces a winter cyclone. Unlike case W1, however, its development occurs predominantly over land. Its $\Delta x = 80$ km and $p_\mathrm{t} = 10$ hPa are identical to those for case W1.

Case S1 begins 00 UTC 12 June 1989 and ends 24 h later. It is dominated by two regions of precipitation: a convective region stretching between New Mexico and Tennessee, and a non-convective region stretching between Southern Manitoba and Lake Michigan. Its dynamics, measured in terms of both wind and temperature gradients, are much weaker than in the winter cases. The horizontal grid spacing for this case is 80 km and $p_\mathrm{t} = 100$ hPa.

Case S2 begins 1200 UTC 16 June 1997 and ends 24 h later. It is dominated by a region of non-convective precipitation over New England, and a region of convective precipitation along a frontal band stretching between Texas and Pennsylvania. Its $\Delta x = 80$ km, but $p_\mathrm{t} = 10$ hPa.

Sensitivities of J_ζ are examined only for the winter cases since our primary interest is actually in the precipitation measures. Fields of ζ on the $\sigma = 0.925$ surface at hour 24 of the two forecasts appear in Fig. 1. The regions where J_ζ is measured are indicated by the squares in the figures. These are centered on the points of minimum surface pressure within the respective cyclones.

In case W1, the maximum ζ is approximately 4×10^{-4} s^{-1}, and large values occur throughout most of the troposphere, so that $J_\zeta = 7.3 \times 10^{-5}$ s^{-1}. In case W2, the maximum ζ within the cyclone is approximately 1.2×10^{-4} s^{-1} and significant vorticity extends only within the range $\sigma > 0.5$, so that $J_\zeta = 3.9 \times 10^{-5}$ s^{-1} Both the structures and intensities of the cyclones in the two cases are therefore different.

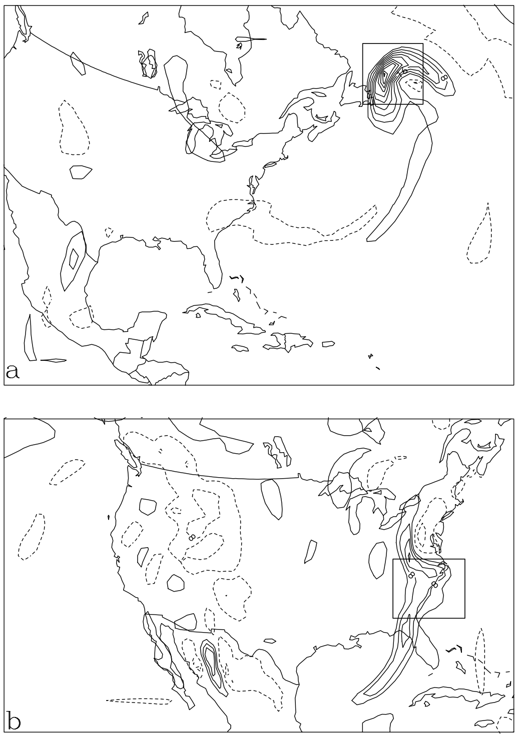

Fig. 1. The forecast ζ on the $\sigma = 0.925$ surface at hour 24 of the forecasts for cases (a) W1 and (b) W2. The contour interval is 4×10^{-5} s^{-1}. The locations where J_ζ are calculated for the two cases are shown in the respective figures as the large squares.

Fields of R_N at hour 24 for the four forecasts are presented in Fig. 2. The region within which J_N is measured for each case is indicated with the corresponding field. Values of J_{N} for cases W1, W2, S1, and S2 are (in kg m^{-2} d^{-1}) 28.2, 29.8, 28.7 and 38.7, respectively. Note that not all the points in the region where R_{N} is measured are precipitating ones.

Fields of R_{C} at forecast hour 24 are shown in Fig. 3, with boxes for the respective J_{C} indicated. Values of J_{C} for cases W1, W2, S1 and S2 are (in kg m^{-2} d^{-1}) 12.1, 15.3, 11.2 and 48.4, respectively.

4. Magnitudes of sensitivities

The impact of a perturbation on a forecast aspect depends not only on the sensitivity of that aspect but also on the magnitude and structure of the specific perturbation. It is therefore non-trivial to discern the general relative importance of perturbation fields from consideration of their corresponding sensitivity fields alone. This is most obviously true when fields have different physical units, so that their corresponding sensitivity fields have different units (e.g., consider comparing $\partial J_{\mathrm{N}}/\partial\zeta = 6 \times 10^{-1}\,\mathrm{kg\,m^{-2}\,d^{-1}\,s^{-1}}$ with $\partial J_{\mathrm{N}}/\partial T = 2 \times 10^{-5}\,\mathrm{kg\,m^{-2}\,d^{-1}\,K^{-1}}$). Even for a single field, however, it may be unreasonably restrictive to consider a single, typical perturbation magnitude at all locations; e.g., a perturbation value of 10^{-3} for q would be unreasonably large for perturbations high in the atmosphere, but 10^{-7} would be extremely small for q perturbations near the surface. Furthermore, not just magnitudes but also reasonable structures (e.g., spatial scales) of perturbations should be considered when estimating importance.

While appropriate magnitudes of perturbations for the dynamic fields, e.g. based on the variance of their initial errors, do not have as great a vertical variation as for the q field, such vertical variation may still be significant. For this reason, a simple but meaningful presentation of magnitudes of sensitivity should at least discern the vertical distribution of those magnitudes. The root-mean-square (rms) values of the sensitivity fields are therefore presented in this section as functions of σ. This will be denoted by a tilde ($\tilde{}$) atop the field symbol, with a subscript indicating which J is being considered; e.g., the rms value of $\partial J_\zeta/\partial T$ will be denoted $\tilde{T}_\zeta$. Consideration of further details of the spatial structures of appropriate perturbations appears in the section on impacts.

It is possible to meaningfully compare values of $\tilde{\zeta}$ and $\tilde{\delta}$. Comparison between those and rms values of either $\tilde{T}$ or $\tilde{q}$ are not possible, however, without further constraints applied. Comparisons of the latter kind will therefore be postponed until the section on impacts. Consideration of the differences in appropriate perturbation magnitudes for ζ and δ fields for comparison of their respective fields of sensitivity will also be postponed until then.

4.1. *Sensitivity of* J_ζ

At $t = 0$, J_ζ is only sensitive to ζ. This sensitivity is only nonzero within the verification box and is identical on all σ-surfaces since $\Delta\sigma$ is constant. Only for $-t > 0$ do the dynamics and physics have time to act so other fields can influence J_ζ.

The rms sensitivities of J_ζ as a function of σ at $t = -12$ for case W1 appear in Fig. 4a. Values for $\tilde{\zeta}_\zeta$ are a maximum near the model's top and bottom with

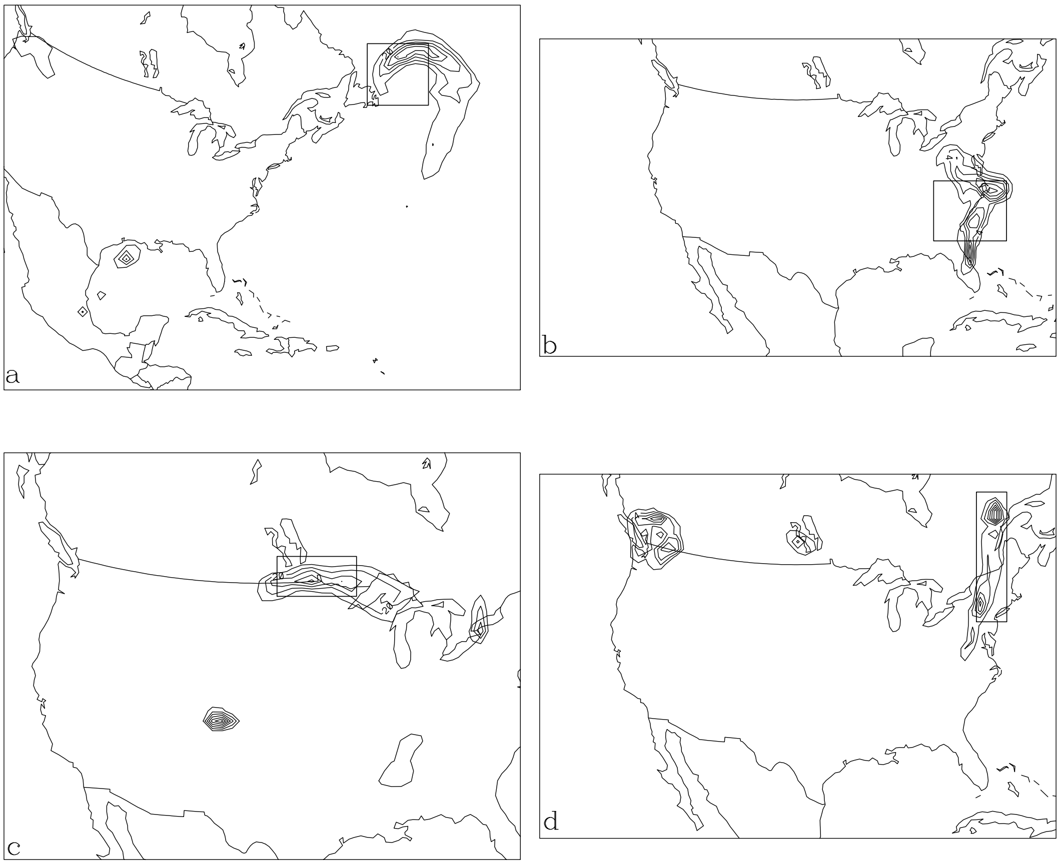

Fig. 2. R_N at hour 24 of the forecasts for cases (a) W1, (b) W2, (c) S1 and (d) S2 with contour intervals 20 kg m^{-2} d^{-1}. The location where J_N is calculated for each case is shown as a rectangle in the respective figures.

a minimum at $\sigma = 0.325$, but with the ratio of maximum to minimum values less than 2.5. This pattern is evident at all $-t \geq 1$, although the exact levels where maximum and minimum values occur, as well as the range between those values, differ slightly. Values for $\tilde{\delta}_\zeta$ are a minimum at the uppermost σ-level, with ratios of maximum to minimum values as large as 5. Values of $\tilde{\zeta}_\zeta$ are more than twice those of $\tilde{\delta}_\zeta$ at the same σ-levels. These ratios are greater at times closer to $t = 0$. The peaks in $\tilde{T}_\zeta$ occur in mid-atmosphere, in agreement with results reported by Langland et al. (1995), Rabier et al. (1996), Klinker et al. (1998), Hoskins et al. (1999) and Gelaro et al. (2000), using the same or other models. The peak in $\tilde{q}_\zeta$ also occurs in mid atmosphere.

Figure 4b is like Fig. 4a, except for case W2. Similarly to case W1, $\tilde{\zeta}_\zeta$ is more than twice $\tilde{\delta}_\zeta$ at all σ-levels, and the peaks in $\tilde{T}_\zeta$ and $\tilde{q}_\zeta$ occur near $\sigma = 0.5$. These peaks are not as dramatic, however, as those for case W1. Furthermore, there is no significant peak in $\tilde{\zeta}_\zeta$ near the model top, and in fact, for $-t > 12$, $\tilde{\zeta}_\zeta$ is a minimum at the topmost σ-level. This may be related to the fact that the dynamics of the reference cyclone for this case are such that the significant forecast vorticity is confined below $\sigma = 0.5$.

In both cases, the maxima of $\tilde{\zeta}_\zeta$, $\tilde{T}_\zeta$ and $\tilde{q}_\zeta$ increase significantly as $-t$ increases. In case W1, the ratios of maxima at $t = -24$ to those at $t = -3$ are 2, 5, and 3 for $\tilde{\zeta}_\zeta$, $\tilde{T}_\zeta$ and $\tilde{q}_\zeta$, respectively. For case W2, these ratios are 2.5, 3 and 2.

The J_ζ sensitivities for case W1 were also computed using the same, diabatically generated reference state, but without considering moisture and its associated physics in the adjoint model. The shapes of the vertical

Fig. 3. As in Fig. 2, except for R_C.

structures of the rms values of the σ-level fields are almost identical to those produced by the moist adjoint model at all times. The ratios of corresponding rms values produced by the moist verses dry versions of the adjoint are near 1 for $-t < 3$, but slowly increase as $-t \to 24$, so that at $t = -24$, the moist values are approximately 25% larger than the corresponding dry ones. This result agrees with related results reported by Errico and Raeder (1999) and Errico et al. (2001) for this case.

4.2. *Sensitivity of precipitation*

The rms values of the J_C sensitivity fields on σ-surfaces at $t = -12$ appear in Fig. 5 for the four cases. They are unlike those for J_ζ in a number of ways. Most notably, for all cases, $\tilde{\zeta}_C$ and $\tilde{\delta}_C$ are very similar at most levels. This is true for all $3 \le -t \le 24$ (not shown), but for $-t < 3$, $\tilde{\delta}_C$ is twice $\tilde{\zeta}_C$ at some levels. For the winter cases (Figs. 5a and b), $\tilde{\zeta}_C$, $\tilde{\delta}_C$ and $\tilde{T}_C$ peak near the surface. This is also true for case S1 for $-t \le 6$. In the summer cases, both $\tilde{T}_C$ and $\tilde{q}_C$ peak in the upper half of the atmosphere ($\sigma < 0.5$). These peaks are observed at nearly the same σ-levels at all t. Peaks of $\tilde{q}_C$ at small σ (e.g. $\sigma < 0.3$) are irrelevant in almost all contexts, since only tiny perturbations should be allowed there, as at high altitudes q itself is always small. For each field, the magnitudes of the maximum σ-surface rms values remain very similar as a function of time for all $1 \le -t \le 24$, except for $\tilde{q}_C$, which decreases by one half between $t = -3$ and $t = -24$.

The rms values of the J_N sensitivity fields on σ-surfaces at $t = -3$ appear in Fig. 6 for the four cases. In many aspects, they are also unlike those for J_ζ but similar to those of J_C. Values of $\tilde{\zeta}_N$ and $\tilde{\delta}_N$ are not very

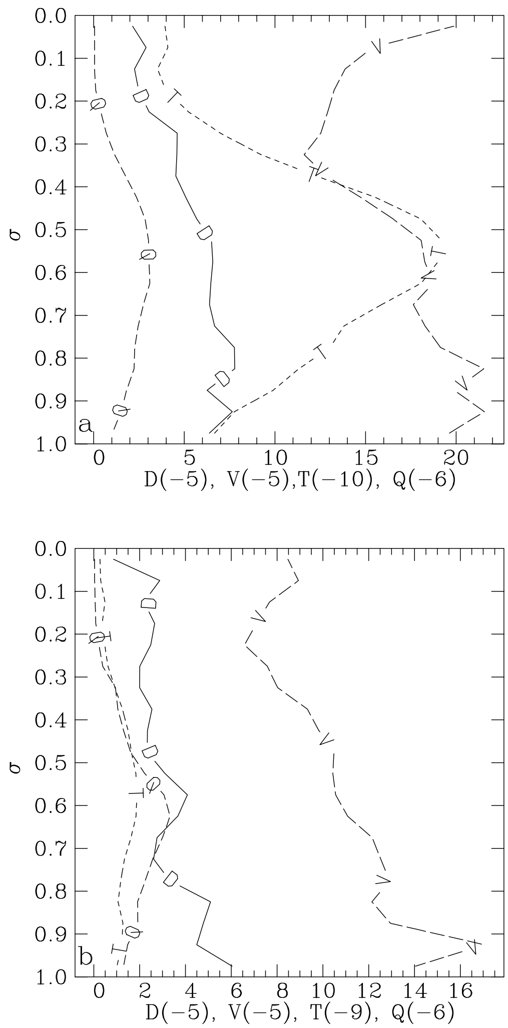

Fig. 4. The rms values of sensitivities of J_ζ as a function of σ and field type (labeled T, Q, V and D for T, q, ζ and δ, respectively). for $t = -12$ h for cases (a) W1 and (b) W2. Values are in units of 10^x s^{-1} K^{-1} for $\tilde{T}_\zeta$, 10^x s^{-1}, for $\tilde{q}_\zeta$, and 10^x for $\tilde{\zeta}_\zeta$ and $\tilde{\delta}_\zeta$, where x is the number in parentheses following each variable at the bottom of the figure.

different at most levels, and for some cases and levels, $\tilde{\delta}_N$ even exceeds $\tilde{\zeta}_N$. In the two winter cases (but especially in W2), both $\tilde{\zeta}_N$ and $\tilde{\delta}_N$ are strongly peaked near the surface. For the summer cases, both $\tilde{T}_N$ and $\tilde{q}_N$ have parabolic-shaped structures in σ, peaking near $\sigma = 0.5$.

Figure 7 is like Fig. 6, except for $t = -12$. There are some significant changes in the vertical structures of the rms sensitivity fields compared with those at $t = -3$. In case S2 (Fig. 7d), $\tilde{\zeta}_N$ is twice $\tilde{\delta}_N$ at many levels, a result that is accentuated as $-t \rightarrow 24$. The peaks near the surface for case W2 seen in Fig. 6b are not as pronounced in Fig. 7b, as the relative importance of $\tilde{\zeta}_N$ and $\tilde{\delta}_N$ for $0.65 < \sigma < 0.9$ have increased. For case S1, $\tilde{T}_N$ for $0.2 < \sigma < 0.5$ exceed those for $\sigma > 0.6$.

Between $t = -3$ and $t = -24$, the maxima of both $\tilde{\zeta}_N$ and $\tilde{\delta}_N$ for cases S1 and W1 decrease by approximately 50% of their respective $t = -3$ values. For case W2, they increase by approximately 100%, but for case S2 they change little. The corresponding changes in the maxima of $\tilde{T}_N$ are smaller for all cases, and there is even less change in the maxima of $\tilde{q}_N$. This result and the similar one for J_C are in contrast to the much greater temporal changes seen for the J_ζ sensitivities, especially regarding both $\tilde{T}_\zeta$ and $\tilde{q}_\zeta$.

Correlations of corresponding sensitivity fields for J_ζ and J_N as a function of field type, σ-level and t were determined for cases W1 and W2. For W1, correlations were generally insignificant, and typically negative valued, implying the two Js are sensitive to different perturbation structures, and for some fields and σ-levels, the same perturbation will increase one J but decrease the other. For W2, correlations are very weak, except for $-t \geq 18$. At $t = -24$, they are general positive and as large as 0.8 at some levels. In this case and time, therefore, identical perturbation structures can significantly impact both J_ζ and J_N.

For case S2, another J was also investigated. This was the convective precipitation accumulated during the final 3 h of the forecast, averaged within the same box as for J_C. The resulting sensitivity structures (but not amplitudes of course) were almost identical to those for J_C. Experiments performed with other cases using a 10-level version of MAMS2 also yielded similar sensitivity structures for rates or corresponding accumulations. Investigating rates rather than accumulations has the advantage that, for t within the period during which accumulations are measured, the magnitudes of sensitivities may be affected by the ability of perturbations to influence only later times and not the entire period of accumulation. For these reasons, we concentrated attention on rates at the end of the forecast rather than on accumulations.

5. Impact measures

The difficulty of comparing sensitivities with respect to diverse fields was described in the previous section. It was argued there that simply claiming that

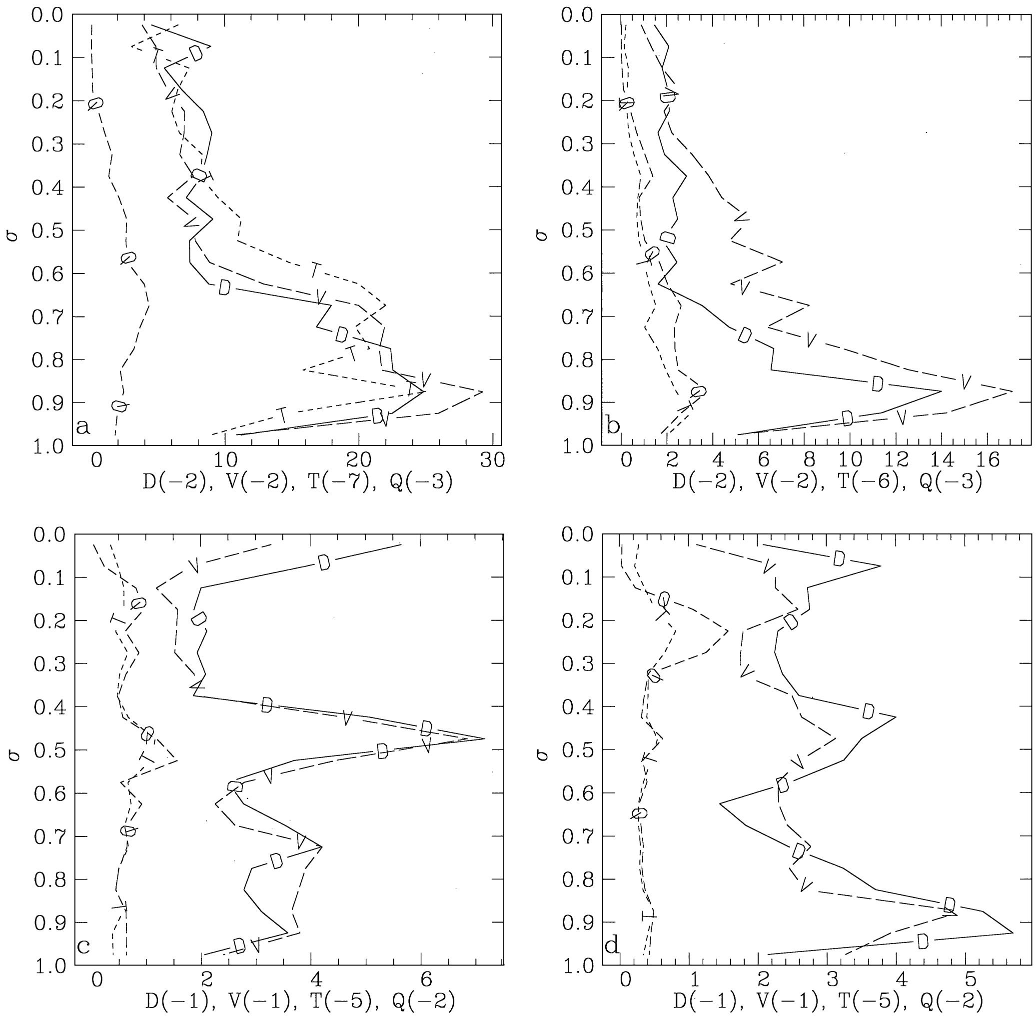

Fig. 5. As in Fig. 4, except for J_C for cases W1, W2, S1 and S2 in (a)–(d), respectively. Values are in units of 10^x kg m^{-2} d^{-1} K^{-1} for $\tilde{\zeta}_C$, 10^x kg m^{-2} d^{-1} for $\tilde{q}_C$, and 10^x kg m^{-2} d^{-1} s for $\tilde{\zeta}_C$ and $\tilde{\delta}_C$.

some number of units of one field are equivalent to some units of another field may be insufficient for comparing diverse fields, most notably other fields with q. Here we therefore use another approach, that of comparing impacts of "optimal" perturbations. These are perturbations of specific magnitude and structure determined from consideration of the corresponding sensitivity field and some additional constraint that is most appropriately based on error covariance statistics for the field. Examples of some classes of such optimal perturbations are described by Rabier et al. (1996), Ortwijn and Barkmeijer (1995), Errico (1997) and Lewis et al. (2001).

Here, optimal perturbations will be independently produced for each type of field examined. Each is determined as the perturbation field $\mathbf{x}'$ (where $\mathbf{x}$ is a vector of grid-point values for any individual field considered) that maximizes

$$J' = \hat{\mathbf{x}}^{\mathrm{T}}\mathbf{x}', \tag{5.1}$$

where $\hat{\mathbf{x}} = \partial J/\partial \mathbf{x}$ and superscript T indicates transpose. The additional imposed constraint is that

$$\beta^2 = \frac{1}{2}\mathbf{x}'^{\mathrm{T}}\mathbf{W}^{-1}\mathbf{x}', \tag{5.2}$$

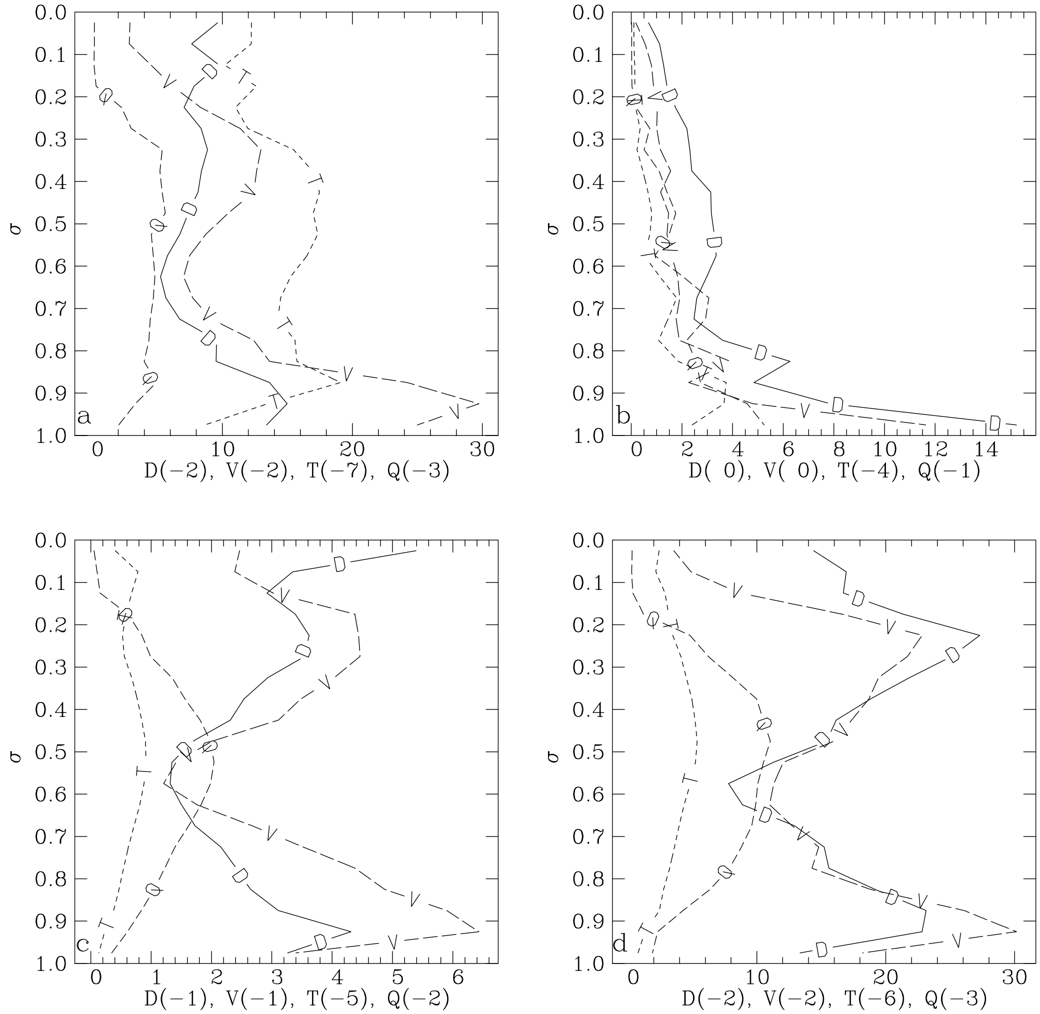

Fig. 6. As in Fig. 4, except for J_{N} at $t = -3$ h for cases W1, W2, S1 and S2 in (a)–(d), respectively. Values are in units of 10^x kg m^{-2} d^{-1} K^{-1} for $\tilde{T}_{\mathrm{N}}$, 10^x kg m^{-2} d^{-1} for $\tilde{q}_{\mathrm{N}}$ and 10^x kg m^{-2} d^{-1} s for $\tilde{\zeta}_{\mathrm{N}}$ and $\tilde{\delta}_N$.

where β is a prescribed constant and $\mathbf{W}$ is a positive-definite, symmetric matrix of weights. Under these constraints, the desired perturbation is

$$\mathbf{x}' = \lambda^{-1}\mathbf{W}\hat{\mathbf{x}}, \tag{5.3}$$

where λ is a Lagrange multiplier:

$$\lambda = \frac{1}{\beta\sqrt{2}}(\hat{\mathbf{x}}^{\mathrm{T}}\mathbf{W}\hat{\mathbf{x}})^{1/2}. \tag{5.4}$$

The impact from such a perturbation is easily estimated by combining eqs. (5.1), (5.3) and (5.4) to yield

$$\mathrm{Max}(J') = \beta\sqrt{2}(\hat{\mathbf{x}}^{\mathrm{T}}\mathbf{W}\hat{\mathbf{x}})^{1/2}. \tag{5.5}$$

Note that $\beta = 1$ can be used without loss of generality for making comparisons between fields, since all results are proportional to that factor.

The comparisons of J' for different fields will depend on the specific $\mathbf{W}$ employed. The appropriateness of any $\mathbf{W}$ depends on the primary application intended for the sensitivities. If the application is data assimilation, a $\mathbf{W}$ derived from background error (typically short-term forecast error) variances (or, better, spatial covariances) is appropriate. If the application is forecast skill estimation or improvement, then a better $\mathbf{W}$ would be analysis (i.e., model initial condition) error

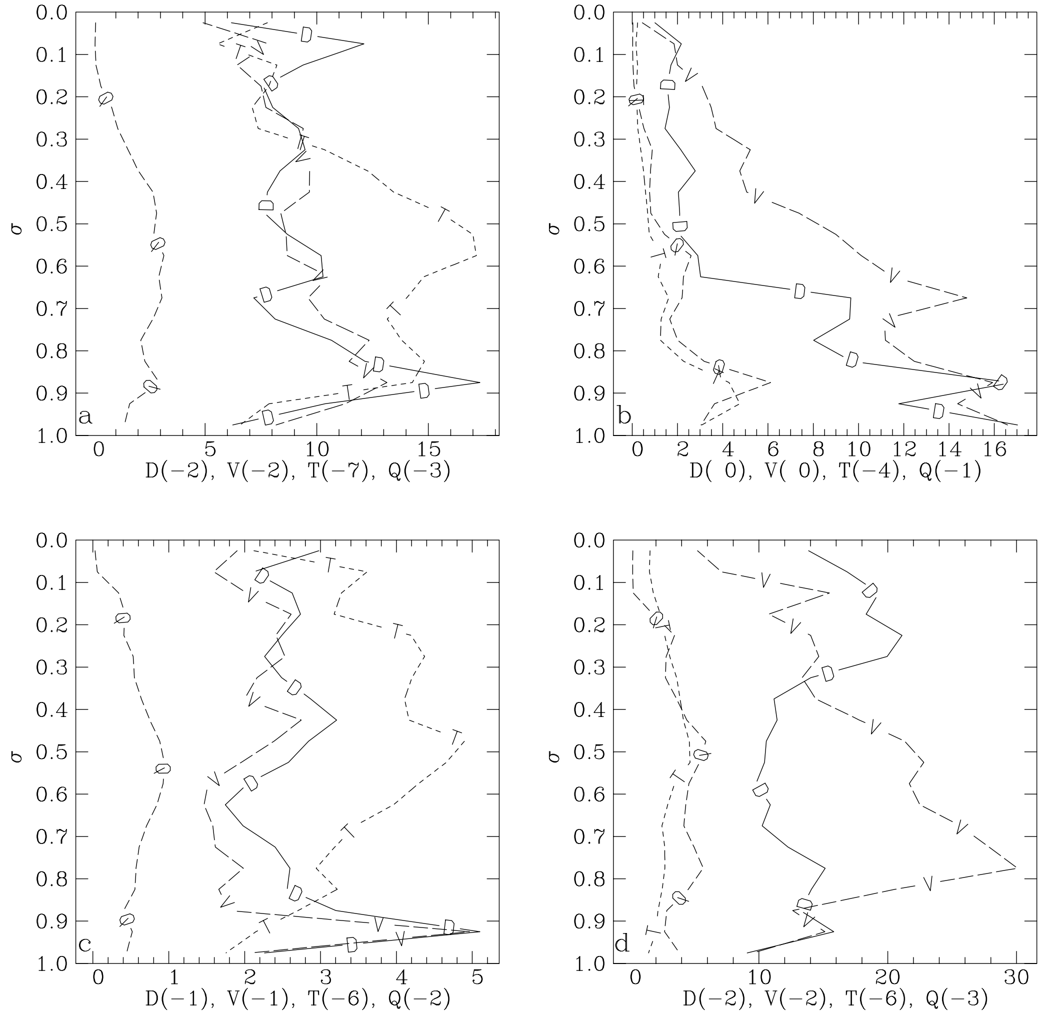

Fig. 7. As in Fig. 6, except $t = -12$.

covariances. These two formulations of **W** may be expected to yield different impacts since, for example, the ratio of the error variance of ζ to that of δ is likely larger for background errors than analysis errors. This is because analysis systems are designed to primarily reduce the largest background errors, which are typically in ζ since it generally has a larger magnitude than δ. Estimates of analysis error covariances are not readily available, however, so a **W** based on analysis error is not an option for us.

The primary **W** used here will be a diagonal matrix whose elements correspond to the values of background (i.e., short-term forecast) error variances presently used for the operational data assimilation system at the Canadian Meteorological Center (CMC). Specifically, these are values for latitude 50°N interpolated to the MAMS2 model levels. They depend on field type and model σ-level.

The diagonal elements of **W** are presented in fig. 8a as a function of σ and field type. In order to present values for all fields in one graph, the values for each field are normalized by the maximum value for that field, so that all curves are confined between 1 and 0. The maximum σ-level variances for the ζ, δ, T and q fields are $6.2 \times 10^{-11}\ \mathrm{s}^{-2}$, $4.3 \times 10^{-12}\ \mathrm{s}^{-2}$, $3.7\ \mathrm{K}^2$ and $9. \times 10^{-7}$, respectively. Note that values for q change

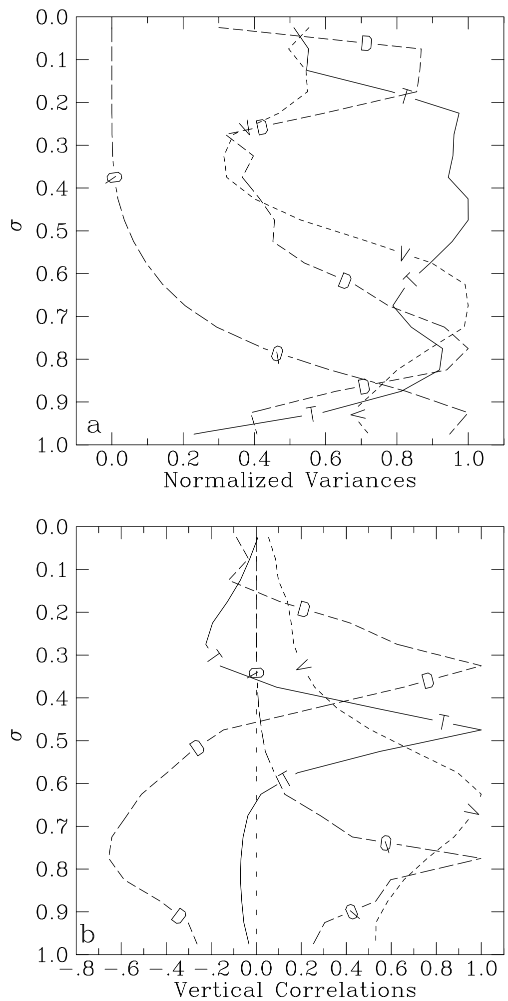

Fig. 8. (a) Normalized variances of fields as function of sigma. (b) Vertical correlations of T (level 10), q (level 16), δ (level 7) and ζ (level 13) with the same respective field at all other levels (labeled as T, Q, D and V, respectively). The variances are normalized by their largest values: 3.7 K^2 for T, 9. $\times 10^{-7}$ for Q, 4.3 $\times 10^{-12}$ s^{-2} for D, and 6.2 $\times 10^{-11}$ s^{-2} for V.

by more than a factor of 100 between $\sigma = 0.925$ and $\sigma = 0.375$. The temperature values are a minimum near the surface, which is unlike values estimated at some other operational weather forecast centers; e.g., see Franke and Barker (2000). The distributions of values for ζ and δ are bimodal, with local maxima occurring in both ranges of $\sigma < 0.2$ and $\sigma > 0.6$.

The optimal perturbations produced using this **W** have horizontal (i.e., σ-surface) structures that are identical to those of the corresponding sensitivity fields but the magnitudes on each level are modified by the corresponding imposed variances. Since these vary vertically, the perturbation structures in the vertical vary differently than the sensitivity field structures. The optimal perturbations are therefore determined similarly to those in Lewis et al. (2001), although with different weighting in the vertical.

Results using the diagonal **W** will be contrasted with those produced using a block diagonal matrix for some experiments. For these, covariances between model levels are considered in addition to the variances on model levels. Specifically the horizontal-scale averaged vertical correlations of background errors at CMC are used to create the covariances. Vertical correlations of ζ or δ are considered identical to those of stream function and velocity potential, respectively. A sample of these vertical correlations are shown in Fig. 8b. Note that for the correlations shown, the one for ζ is always positive valued, but those for other fields have negative-valued lobes. These characterizations are not necessarily representative of those between other levels.

Use of the block diagonal **W** in eq. (5.2) may be interpreted as placing a vertical penalty on structures that are not consistent with the assumed error covariances. Such inconsistency is very plausible, and non-diagonal aspects of **W** may cause qualitative as well as quantitative changes to the impacts (5.5). If significant changes are observed, further significant changes may be obtained by also considering horizontal correlations in defining **W**. The goal here is not really to contrast specific optimal perturbations, however, but to compare more general sensitivity structures: the classes of optimal impacts investigated are intended only as possible means of assessing relative importance of initial perturbations. For these reasons and because much more computation effort is entailed (effectively requiring many components of data assimilation schemes that are not available at NCAR), more complex **W** have not been considered here.

5.1. *Impact results for diagonal* **W**

The independent impacts of optimal perturbations of T, q, ζ and δ on J_ζ as functions of time for cases W1 and W2 appear in Figs. 9a and b, respectively. The optimal perturbation that has the greatest impact on J_ζ for forecast periods longer than 3 h in both cases is that of the T field. Compared with impacts of other perturbation fields, its impact increases at the fastest

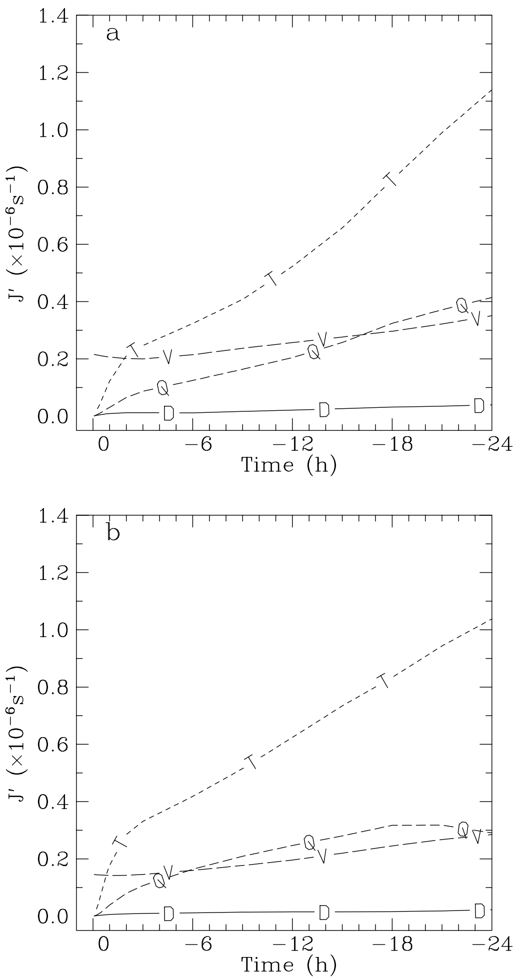

Fig. 9. Impacts on J_ζ due to optimal perturbations of T, q, ζ and δ (curves labeled by T, Q, V and D, respectively) for forecasts begun the indicated hours t before the end of the forecast when J_ζ is measured for cases (a) W1 and (b) W2. Only the diagonal elements of **W** (i.e., error variances but no covariances) are considered.

rate as the forecast duration increases (for case W1, a factor of 4 larger at $t = -24$ compared with the $t = -3$ result). In contrast, those for ζ or δ increase by a factor of 2 or less over the same period. Note that optimal q perturbations at $t = -6$ have about one-half the impact of those of ζ in case W1 but the same impacts in case W2. At longer forecast durations this ratio is larger, such that at $t = -24$, it exceeds those of ζ for both cases. This suggests that, at most times, $\partial J_\zeta/\partial q$ should not be treated as negligible compared with $\partial J_\zeta/\partial\zeta$. In contrast, note that the impact of δ on J_ζ remains several times smaller than that of ζ at all times. This is due to the smaller perturbation sizes permitted for the δ field as well as to the generally smaller values of $\partial J_\zeta/\partial\delta$ compared with those for ζ.

The independent impacts of optimal perturbations of initial fields on J_C for all the cases appear in Fig 10. For all cases, for $-t > 1$, the optimal T perturbation has greater impact than those of other fields. For $-t > 9$, the impacts of q and ζ are almost the same, except for case W2 for which that of q is approximately 30% larger than that of ζ. For $-t > 3$, impacts of ζ are generally 4 or more times larger than those of δ. Impacts of T and q are 3 or more times larger for $-t < 1$ compared with corresponding values for $-t > 6$, but for such short forecast periods, impacts of ζ and δ are near zero. This is not surprising since the convection scheme of Moorthi and Suarez (1992) depends directly only on T and q, not winds, and therefore the winds need more time to act dynamically in order to influence the thermodynamics and hence the convection. In section 7, the surprising result that all the impact curves for $9 < -t < 24$ are rather flat will be addressed.

The independent impacts of optimal perturbations of initial fields on J_N for all cases appear in Fig. 11. In many respects, similar statements apply to these as to those for J_C. In particular, the impacts of T dominate those of other fields, and none of the impact curves, except for ζ in case W2, show large growth as $-t$ increases beyond 6 h. This is very unlike what is observed for J_ζ in Fig. 9.

The regions over which J_ζ was computed were appropriate for the corresponding forecast structures of ζ, but the same regions were chosen for J_N so that, in those cases, regions and forecast aspects were not changed simultaneously. Those regions were not a-priori the best for evaluating J_N, since precipitation did not fill those areas. For this reason, experiment W1 was repeated with the region for computing J_N shifted approximately 500 km to the northeast. Compared with the former experiment, the sensitivities generally increased by 20%, since more precipitating points were present to be measured. Between $t = -9$ and $t = -24$, J_N increased by approximately 50% for optimal T perturbations, but insignificantly for other fields. The results of this experiment are therefore still qualitatively very different from those examining J_ζ, and those differences do not appear to be explained simply by the specific choice of region for originally evaluating J_N.

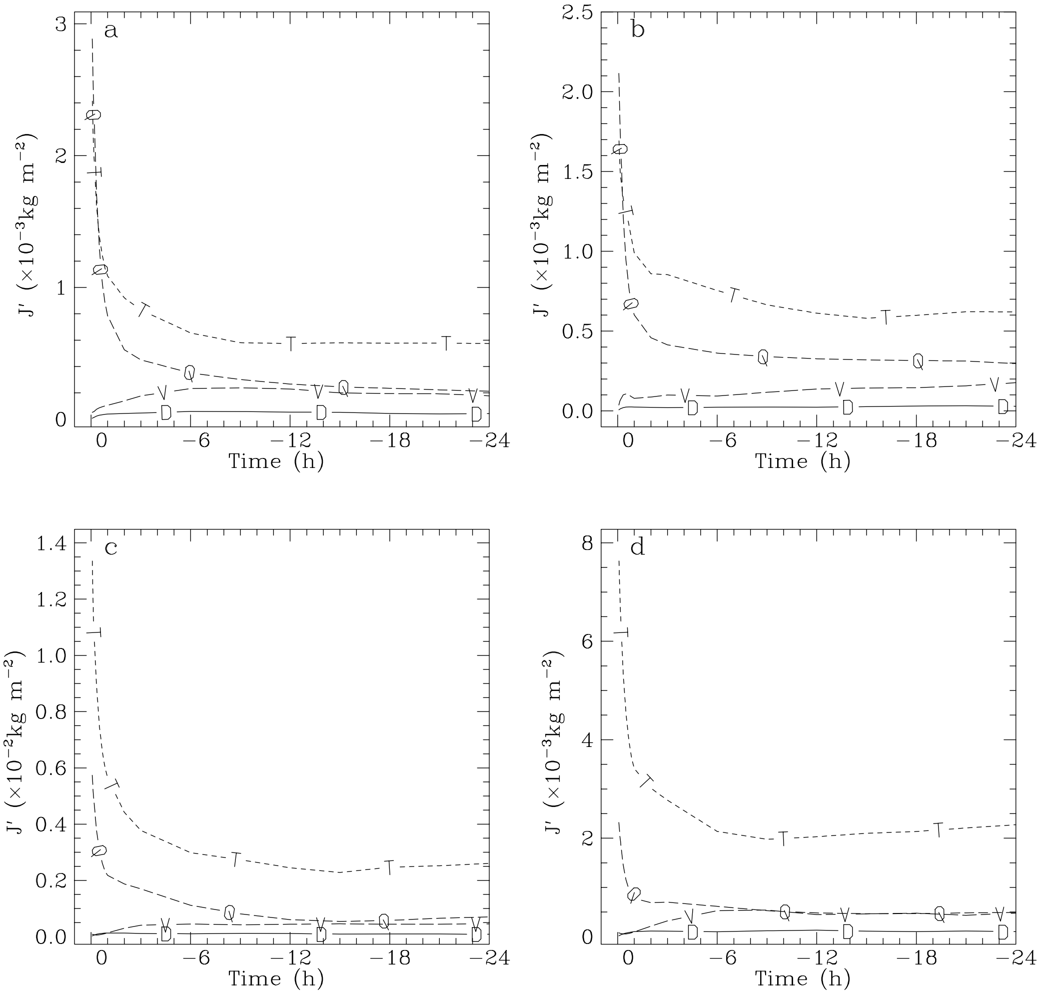

Fig. 10. As in Fig. 9, except for J_C for cases (a) W1, (b) W2, (c) S1, and (d) S2. Time steps 0 and 1 are not plotted here because a large spike in the sensitivity at the first time step would cause the axis scale to be so large that the fields at later times would be difficult to distinguish.

5.2. *Impact results for non-diagonal* **W**

As an example illustrating the effect of considering vertical correlations in the specification of **W**, all the optimal impacts computed for case W2 are presented in Figs. 12a–c using the CMC-derived correlations. These are to be contrasted with the variance-only results shown in Figs. 9b, 10b and 11b, respectively. Little difference is seen for J_C. For J_N, the ordering of the impacts for each field remains the same, but for $-t > 3$, all impacts are slightly increased. The most notable differences, however, are observed for J_ζ: when the correlations are considered, the impact of ζ is greater than that of q, with the former more than doubled compared to its variance-only value. This is because $\partial J_\zeta / \partial \zeta$ has a strong barotropic component (as revealed by further detailed examination) that projects strongly on the leading principal components of the matrix of vertical covariances for vorticity.

6. Test of linearity

Proper interpretation of adjoint-derived sensitivities requires ensuring that, for applications of interest, the

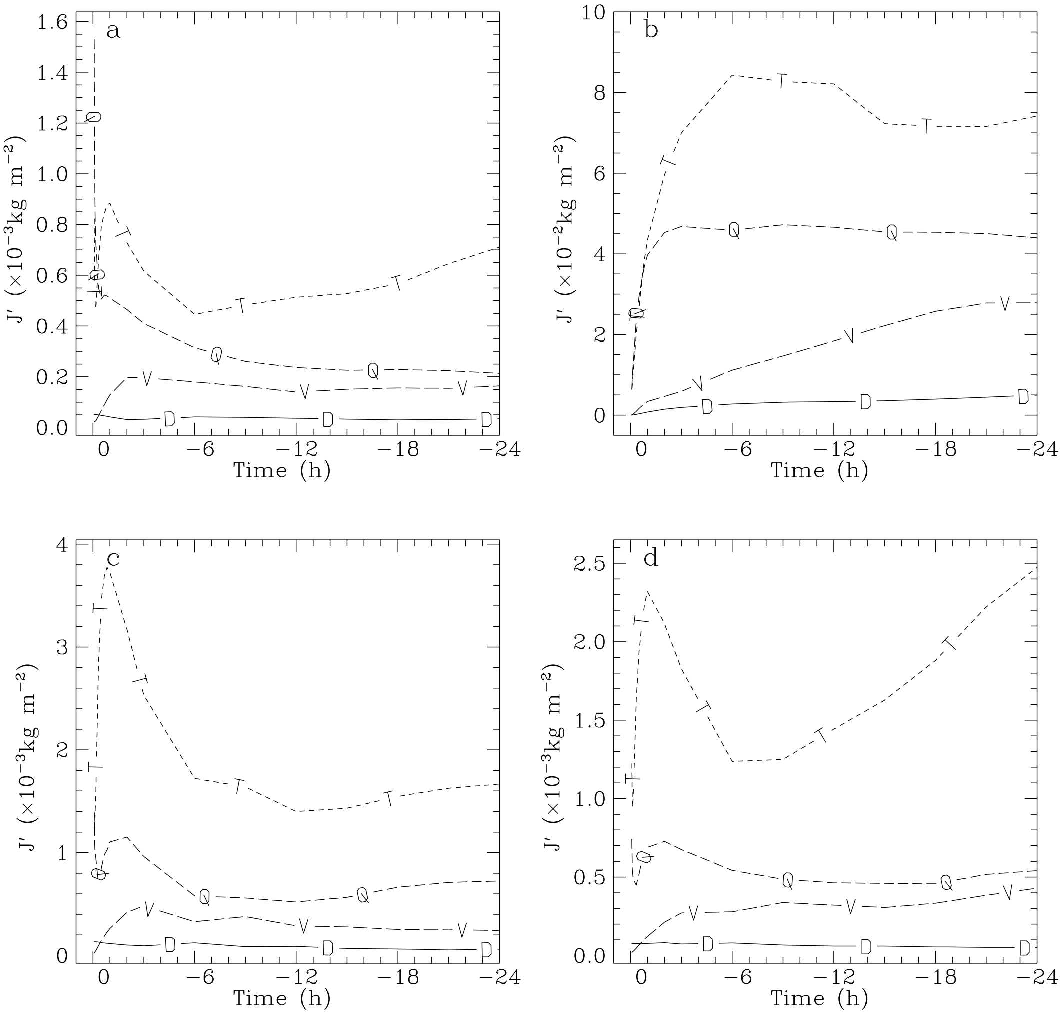

Fig. 11. As in Fig. 9, except for J_N for cases (a) W1, (b) W2, (c) S1, and (d) S2.

behavior of meaningful perturbations are indeed quasilinear (Errico et al., 1993; Errico, 1997). This is especially necessary when highly nonlinear precipitation processes are being considered (Errico and Raeder, 1999).

We are not considering any specific application here, although one of our concerns is data assimilation. Since we do not possess a data assimilation system for MAMS2, however, it is difficult for us to directly consider applications to such problems. Instead, therefore, we consider the nonlinear behavior of the optimal perturbations that we employed to compare impacts.

The choice of value for β, which defines the magnitudes of the optimal perturbations, can have a profound effect on the agreement between linear and nonlinear impacts. Because β is proportional to a measure of perturbation size averaged over the entire model domain, whereas the sensitivity structures are typically very localized, it is awkward to assign a reasonable value to β without considering the specific sensitivity structures that define the shapes of the perturbations. Instead, therefore, we designate a value of β for each case by determining what that value must be in order to obtain a maximum perturbation of q equal to 1 g kg^{-1} for its J_C optimal. That same β is then used for all fields. It should be noted that this scaling implies that all but one grid-point value of q' are less than 1 g kg^{-1} and that typical or rms values of q' are much smaller

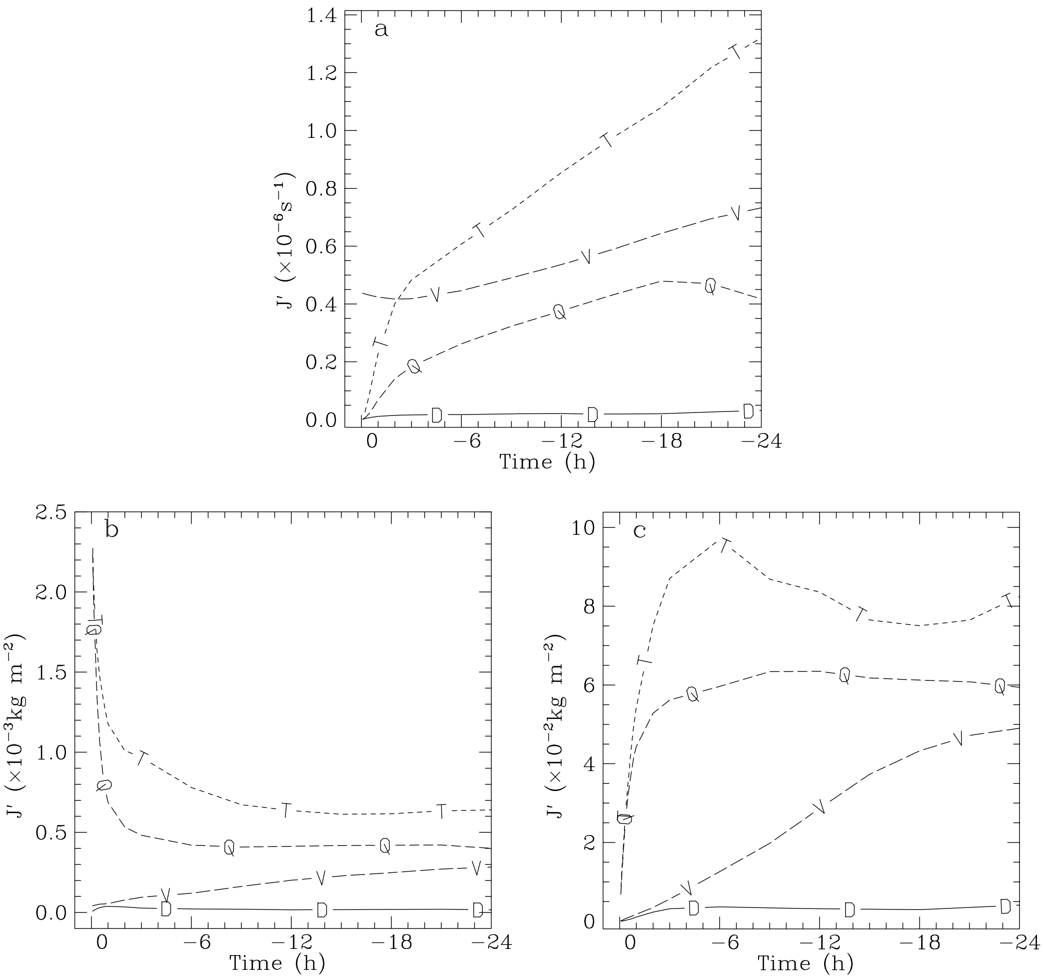

Fig. 12. As in Fig. 9, except for (a) J_ζ, (b) J_C and (c) J_N for case W2 considering vertical covariances of each individual field in the definition of **W**.

than 1 g kg^{-1}, with corresponding implications applying to the other fields. The impacts of these optimal perturbations as they have been scaled are therefore not necessarily great.

Values of J' for selected cases, forecast aspects and fields perturbed appear in Table 1. Corresponding nonlinear results ΔJ as well as the unperturbed reference forecast values of J all appear for comparison. Only optimal perturbations of q and ζ were examined in these tests. No results are presented for case W1, since similar tests for it are described in Errico and Raeder (1999).

Values for $J = J_\zeta$ for case W2 appear in row 1 of Table 1. These are for 24 h forecasts, for which the reference J_ζ is 3.9×10^{-5} s^{-1}. In accordance with Fig. 9b, the linear estimate of the impact of the optimal q' is greater than that of ζ'. This ordering is not observed in the nonlinear result, where for the optimal q' the nonlinear result has been reduced by 30% compared to the linear result, but for the optimal ζ', the reduction is only 6%. The large ratio between linear and nonlinear values for the q' experiment indicates that nonlinear effects are significant. So for this case and rather long (24 h) time period, the linear (adjoint) estimates are quantitatively unreliable.

Results for case W2 and $J = J_C$ appear in row 2 of Table 1. The reference $J_C = 15$ kg m^{-2} d^{-1}. Nonlinear results for optimal q' and ζ' are only reduced by

Table 1. *Comparison of linear* J′ *(LIN) and nonlinear* J′ *(NL) impacts produced by optimal perturbations of vorticity and* q *for the indicated cases and forecast aspects*

		Vorticity perturbation			Moisture perturbation		
Case	BS J	LIN J'	NL J'	Ratio	LIN J'	NL J'	Ratio
W2	$J_V = 38.9$	2.34	2.20	1.06	2.50	1.73	1.45
W2	$J_C = 1.53$	0.265	0.240	1.10	0.439	0.367	1.20
S1	$J_C = 1.12$	0.837	0.616	1.36	1.40	0.972	1.44
S2	$J_C = 4.84$	1.11	0.215	5.16	1.18	0.400	2.95
S26	$J_C = 3.90$	0.651	0.573	1.14	0.775	0.643	1.21

The ratios (LIN J'/NL J') for corresponding impacts are also presented along with the reference values of (BS) of J. All values are for 24 h forecasts, except for the case labeled S26, which is for a 6 h forecast of case S2. Units of $\mathbf{J_v}$ are 10^{-6} s^{-1} and units of $\mathbf{J_c}$ are 10 kg m^{-2} d^{-1}.

18% and 10% of their respective linear results. The ordering of the impacts is the same in both linear and nonlinear estimates. No significant nonlinear effects are indicated by these numbers.

Results for 24 h forecasts of J_C for the summer cases appear in rows 3–4. The discrepancies between J' and ΔJ are factors of between 1.4 and 5.2. These indicate that the summer adjoint results are unreliable for forecasts as long as 24 h and initial perturbations as large as used, unless factors of two for $J'/\Delta J$ are acceptable. These discrepancies are only slowly reduced as β is reduced by a factor of 20.

The discrepancies are greatly reduced, however, if shorter forecast periods are considered. Row 5 is one example of the latter, determined for a 6 h forecast of case S2 valid at the same concluding time. (The difference in J_C reported in rows 4 and 5 is due to the 6-h forecast beginning with a forward time step, rather than a centered one as in the 24-h forecast, as well as to slight changes in the boundary conditions for the 6 and 24-h forecasts.) For the 6-h forecast, the $J'/\Delta J$ are 1.21 for q' and 1.14 for ζ'. These ratios are very close to 1 considering that J is a nonlinearly determined precipitation rate and that quasi-linear dynamics are relatively weak in case S2. These results agree with those of complimentary tests performed by Errico and Raeder (1999) using the same model.

7. Conclusions

Although examination of the sensitivity of measures of vorticity was not a goal of this work, it was examined here to provide a contrast to the sensitivities of precipitation rates. The measure used was barotropic vorticity averaged within an area centered on cyclones in two winter cases. In order to compare sensitivities of distinct fields, optimal perturbation were considered using weights based on 6-h forecast error variances. In agreement with adjoint results reported by others (e.g., Langland and Errico, 1995; Langland et al., 1995; 1996), for forecasts longer than 3 h, barotropic vorticity was most sensitive to possible initial temperature perturbations, with that sensitivity peaking near or below mid-troposphere. Additionally, rms sensitivity to initial perturbations of vorticity was several times larger than that due to divergence, with the peak in sensitivity to vorticity occurring low in the atmosphere for forecasts longer than 12 h. For some forecast lengths, an additional relative maximum in the sensitivity to vorticity occurred near the model top, with a minimum near the 300 hPa surface.

Surprisingly, significant sensitivity of barotropic vorticity to the initial moisture field was also found for forecasts longer than several hours. This was true not only for an explosively deepening, diabatically enhanced oceanic cyclone but also for a more typical continental cyclone.

The sensitivity of barotropic vorticity with respect to initial temperature perturbations increased rapidly as longer forecast times were considered. On most σ-surfaces, the rms values of sensitivity with respect to initial temperature perturbations increased by 300% or more between forecast durations of 3 and 24 h. The sensitivity with respect to other initial fields also increased as longer forecast times were considered, but not as rapidly as the sensitivity with respect to temperature.

The sensitivities of both convective and non-convective precipitation with respect to model initial perturbations were similar in many respects, but very different than the sensitivities of vorticity. The rms sensitivities with respect to initial vorticity and divergence were similar to each other on most model surfaces, although in some cases, for forecast periods longer than 12 h, sensitivity to vorticity was greater than that to divergence.

For forecasts longer than 1 h, the precipitation impacts of optimal perturbations whose weights are determined by background error variances are greatest for temperature perturbations, then next greatest for moisture perturbations followed by vorticity perturbations. Although sensitivities to divergence and vorticity are similar, the weights allow greater magnitudes of vorticity perturbations than of divergence, and therefore the impacts of divergence perturbations are smallest.

For different forecast aspects associated with the same feature, such as vorticity or precipitation associated with the same cyclone, we expected that the sensitivities of those aspects would vary similarly in time. In particular, we expected the sensitivities of precipitation measures to increase with forecast duration as those of vorticity. Essentially the longer the forecast duration, the more time perturbations have to grow. Of course, in the nonlinear model, precipitation, unlike vorticity, is limited by moisture availability, but the adjoint-estimated sensitivities do not account for this constraint.

Unexpectedly therefore, the rms magnitudes of the precipitation sensitivity fields did not increase greatly as longer forecast periods were considered, in contrast to the behavior of barotropic vorticity sensitivity. Examination of correlations of corresponding sensitivity structures or experimentation with shifting the region over which precipitation was measured did not offer us insight into the cause of this difference. Perhaps, however, it was simply that the two measures, although associated with the same synoptic feature, actually concerned only weakly coupled aspects. This hypothesis should be tested further by someone acquainted with the problem from a synoptics viewpoint who is otherwise willing to learn use of powerful adjoint tools.

The primary results here are that moisture errors can significantly affect vorticity forecasts in developing cyclones and that 3–24 h precipitation forecasts can be significantly affected by temperature errors. These results warrant confirmation in other models and further investigation in general. There are many other interesting aspects of these results, for example, regarding the vertical distributions and temporal variations of sensitivities that also warrant further investigation. We welcome others who are interested to attempt to interpret our results synoptically.

8. Acknowledgments

This work was partially supported by the U.S. Navy Office of Naval Research grant numbers N00173-96-MP-0086 and N00014-99-1-0017, the U.S. National Aeronautics and Space Administration grant number W-18,077, Mod. 6, and the United States Weather Research Program. We thank Rolf Langland, Ron Gelaro, and two anonymous reviewers for their comments on earlier versions of this manuscript.

The National Center for Atmospheric Research is sponsored by the U.S. National Science Foundation.

REFERENCES

Anthes, R. A., Kuo, Y.-H., Baumhefner, D. P., Errico, R. M. and Bettge, T. W. 1985. Predictability of mesoscale motions. *Issues in Atmospheric and Oceanic Modeling, Part B, Adv. Geophys.* **28**, 159–202.

Bourke, W. and McGregor, J. L. 1983. A nonlinear vertical mode initialization scheme for a limited area prediction model. *Mon. Wea. Rev.* **111**, 2285–2297.

Davies, H. C. and Turner, R. E. 1977. Updating prediction models by dynamical relaxation: An examination of the technique. *Q. J. R. Meteorol.* **103**, 225–245.

Ehrendorfer, M., Errico, R. M. and Raeder, K. D. 1999. Singular-vector perturbation growth in a primitive-equation model with moist physics. *J. Atmos. Sci.* **56**, 1627–1648.

Errico, R. M. 1997. What is an adjoint model. *Bull. Am. Meteorol. Soc.* **78**, 2577–2591.

Errico, R. M. 2000a. Interpretations of the total energy and rotational energy norms applied to determination of singular vectors. *Q. J. R. Meteorol. Soc.* **126A**, 1581–1599.

Errico, R. M. 2000b. The dynamical balance of singular vectors in a primitive equation model. *Q. J. R. Meteorol. Soc.* **126A**, 1601–1618.

Errico, R. M. and Baumhefner, D. P. 1987. Predictability experiments using a high-resolution limited-area model. *Mon. Wea. Rev.* **115**, 488–504.

Errico, R. M. and Raeder, K. D. 1999. An examination of the accuracy of the linearization of a mesoscale model with moist physics. *Q. J. R. Meteorol. Soc.* **125**, 169–195.

Errico, R. M. and Vukićević, T. 1992. Sensitivity analysis using an adjoint of the PSU-NCAR mesoscale model. *Mon. Wea. Rev.* **120**, 1644–1660.

Errico, R. M., Vukicevic, T. and Raeder, K. 1993. Examination of the accuracy of a tangent linear model. *Tellus* **45A**, 462–497.

Errico, R. M., Raeder, K. and Vukićević, T. 1994. *Description of the NCAR Mesoscale Adjoint Modeling System version 1 (MAMS1).*NCAR Technical Note, NCAR/TN–410+IA. (Available from the National Center for Atmospheric Research, P.O. Box 3000, Boulder, CO 80307, USA.)

Errico, R. M., Ehrendorfer, M. and Raeder, K. D. 2001. The spectra of singular values in a regional model. *Tellus* **53A**, 317–332.

Franke, R. and Barker, E. 2000. Vertical correlation functions for temperature and relative humidity errors. *Mon. Wea. Rev.,***128**, 3962–3981.

Gelaro, R., Reynolds, C. A., Langland, R. H. and Rohaly, G. D. 2000. A predictability study using geostationary satellite wind observations during NORPEX. *Mon. Wea. Rev.* **128**, 3789–3807.

Hall, M. C. G., Cacuci, D. G. and Schlesinger, M. E. 1982. Sensitivity analysis of a radiative convective model by the adjoint method. *J. Atmos. Sci.* **39**, 2083–2050.

Hoskins, B. J., Buizza, R. and Badger, J. 1999. The nature of singular vector growth and structure. *Q. J. R. Meteorol. Soc.* **126**, 1565–1580.

Klinker, E., Rabier, F. and Gelaro, R. 1998. Estimation of key analysis errors using the adjoint technique. *Q. J. R. Meteorol. Soc.* **124**, 1909–1933.

Langland, R. H. and Errico, R. M. 1995. Comments on "Use of an adjoint model for finding triggers for Alpine lee cyclo-genesis." *Mon. Wea. Rev.* **124**, 757–760.

Langland, R. H., Elsberry, R. L. and Errico, R. M. 1995. Evaluation of physical processes in an idealized extratropical cyclone using adjoint sensitivity. *Q. J. R. Meteorol. Soc.* **121**, 1349–1386.

Langland, R. H., Elsberry, R. L. and Errico, R. M. 1996. Adjoint sensitivity of an idealized extratropical cyclone with moist physical processes. *Q. J. Roy. Meteorol. Soc.* **122**, 1891–1920.

Lewis, J., Raeder, K. D. and Errico, R. 2001. Vapor flux associated with return flow over the Gulf of Mexico: A sensitivity study using adjoint modeling. *Tellus* **53A**, 74–93.

Moorthi, S. and Suarez, M. J. 1992. Relaxed Arakawa–Schubert: A parameterization of moist convection for general circulation models. *Mon. Wea. Rev.* **120**, 978–1002.

Mullen, S. L. and Baumhefner, D. P. 1989. The impact of initial condition uncertainty on numerical simulations of large-scale explosive cyclo-genesis. *Mon. Wea. Rev.* **117**, 2800–2821.

Oortwijn, J. and Barkmeijer, J. 1995. Perturbations that optimally trigger weather regimes. *J. Atmos. Sci.* **52**, 3952–3944.

Rabier, F., Klinker, E., Courtier, P. and Hollingsworth, A. 1996. Sensitivity of forecast errors to initial conditions. *Q. J. R. Meteorol.* **122**, 121–150.

Stensrud, D. J., Bao, J.-W. and Warner, T. T. 2000. Using initial condition and model physics perturbations in short-range ensembles of mesoscale convective systems. *Mon. Wea. Rev.* **128**, 2077–2107.